Supporting Information for: Holocene Formation of Henry Ice Rise, West Antarctica, Inferred from Ice-Penetrating Radar

Martin G. Wearing [1], Jonathan Kingslake [1]

[1]Lamont-Doherty Earth Observatory, Columbia University, New York, USA

Contents of this file

Introduction

Here we provide additional details and examples of the dating technique described in the main text. We also present ice-divide transects that show the absence of Raymond Arches.

1) Determining Accumulation Rate and Associated Uncertainty over Henry Ice Rise

A key parameter used to determine the age of relic crevasses within Henry Ice Rise (HIR) is the surface accumulation rate. We consider estimates from a remote-sensing product, which uses the polarization of microwave emissions (Arthern, Winebrenner, & Vaughan, 2006), and a regional climate model RACMO2.3p2 (van Wessem et al., 2018), to determine the surface accumulation rate at our site. Figures 1a and b show the variation in accumulation rate within 100 km radius of the northern promontory of HIR, from Arthern et al. (2006) and van Wessem et al. (2018) respectively. Figure 1c shows the normalized frequency distribution of these accumulation rates. The modal accumulation varies systematically between the two methods; 120 kg m^{-2} yr^{-1} from RACMO and 160 kg m^{-2} yr^{-1} from Arthern et al. (2006). We include the uncertainty from these measurements, with an accumulation rate centred at 140 kg m^{-2} yr^{-1} with a range of $\pm$ 40 kg m^{-2} yr^{-1} (0.153 ± 0.044 m yr^{-1}). This covers the range from the two methods. Figure 1d shows the normalized variation in accumulation back from present day from the WAIS Divide ice core (Koutnik et al., 2016), with an additional line indicating the average between 0 and 6 kyr BP. This normalized history of accumulation is used in Section 6 to evolve in time the accumulation rate at HIR.

The spatial variation in accumulation rate centred between the Doake Ice Rumples (DIR) and the downstream radar profile for radii 50, 100 and 200 km is shown in Figure 1e. Here we estimate the accumulation rate using the median value from the distribution, which is 165 kg m^{-2} yr^{-1} (0.18 m yr^{-1}).

2) Low Amplitude Arches and Age Estimates

Here we present additional figures demonstrating the occurrence and location of low amplitude arched isochrones, possible proto-Raymond Arches (Figures 2 and 3), along with the age of relic basal crevasses at example locations (Figure 2), calculated using the technique detailed in the main text.

3) Absence of Raymond Arches over Southern Divides

From radargrams traversing ice-divides in the southern sections of HIR (Figure 4) it is evident that these divides have not been stable for long periods (in comparison to the characteristic time 4.6 kyr) due to the absence of Raymond Arches.

4) Example of Dating Method for Line B_3 West Flank

Figure 5 shows the values extracted from the B_3 radar profile to date the initial advance of the ice rumple (Stage 4 - 5): bed elevation (-541 m above sea level (a.s.l.)), relic crevasse height (-417 m a.s.l.) and surface height (87 m a.s.l.).

Figure 6 shows the evolution of the ice thickness, H, relic crevasse height, surface vertical velocity, w_s and crevasse-capping isochrone vertical velocity, w, for ten runs of the Monte-Carlo simulation, used to estimate the age of initial advance on the West Flank along line B_3. The mean age from these ten simulations is 6.8 kyr with a standard deviation of 2.0 kyr.

From the time-evolution of the ice thickness (Figure 6a) it is possible to see the influence of the uncertainty in the radar measurements, the GIA rate and the thickness-change parameter β. The uncertainty in the GIA rate and different estimated ages leads to the range in initial ice thickness (the thickness at which the basal crevasses grounded). The thickness change parameter determines the slope from initial grounding to present-day, with a range of profiles from convex, through linear, to concave, each ending at the present-day thickness of 638 $\pm$ 6 m (uncertainty in radar measurement plus vertical GPS measurement). In this location the ice thins between initial grounding and present-day.

Our simulations consider basal crevasses that are 40% $\pm$ 15% of the initial ice thickness. Therefore, there is a range in initial crevasse height, due to this and the variation in initial ice thickness. For these 10 simulations, the largest basal crevasse is approximately 390 m (corresponding to initial ice thickness of approximately 740 m and an initial basal crevasse height of approximately 53% of the ice thickness). The smallest basal crevasse is approximately 200 m in height (corresponding to an ice thickness of approximately 690 m, 29% of the ice thickness). In all cases, the downward propagation of the top of the relic crevasse decreases in time as the crevasse is buried, Figure 6d.

Surface accumulation is kept constant during each simulation but allowed to vary between simulations (0.153 $\pm$ 0.044 m yr^{-1}). Vertical velocities at the surface correspond to the time derivative of the thickness. Therefore, when the thickness derivative increases in time (i.e. becomes more positive; purple curve) the magnitude of the vertical surface ve-

locity decreases (slower downward flow). Whereas, for thickness derivatives that decrease in time (dark blue) the magnitude of the surface velocity increases (faster downward flow).

5) Age Estimates over Northern Promontory

See Figure 7 for dating estimates along radar profiles at the north of HIR.

6) Age Estimates for Varying Accumulation History

Figure 8 shows the frequency distribution of age estimates for varying parameterizations of the accumulation rate for the most upstream basal crevasse on line A_1. When the accumulation rate varies in time according to the normalized scaling from the WAIS Divide ice core (WDC) (Figure 1d) there is an average increase of 11% in the past 6 kyr. This leads to slightly younger age estimates as the basal crevasse is buried at a faster rate. The orographic effect is small and when ages are rounded to the nearest 100 yr, in this case, there is no change in the age estimate. Comparing Figure 8a and e, as well as, Figure 8b and c, shows that when accumulation scales with the WDC there is a decrease in the mean age estimate by 500 yr. However, the standard deviation remains fairly unchanged as there is still large uncertainty in the present-day accumulation rate.

7) Convergence of Mean and Standard Deviation in Monte Carlo Procedure

Figure 9 shows the spread in mean age and standard deviation from 10 instances of the Monte Carlo process. The number of runs included within each Monte Carlo process is varied by factors of 10. This calculation is performed for the most upstream relic basal crevasse on the west flank of line B4. The spread in both the mean and standard deviation decreases as the number of runs is increased. For 20,000 runs (purple circles) the range of means ages has reduced to 50 yr and the range in standard deviations has reduced to 30 yr. This number of runs is used for the calculations in the main text.

References

Arthern, R. J., Winebrenner, D. P., & Vaughan, D. G. (2006). Antarctic snow accumulation mapped using polarization of 4.3-cm wavelength microwave emission. *Journal of Geophysical Research*, *111*(D6), D06107. Retrieved from http://doi.wiley.com/10.1029/2004JD005667 doi: 10.1029/2004JD005667

Koutnik, M. R., Fudge, T. J., Conway, H., Waddington, E. D., Neumann, T. A., Cuffey, K. M., ... Taylor, K. C. (2016, may). Holocene accumulation and ice flow near the West Antarctic Ice Sheet Divide ice core site. *Journal of Geophysical Research: Earth Surface*, *121*(5), 907–924. Retrieved from http://doi.wiley.com/10.1002/2015JF003668 doi: 10.1002/2015JF003668

van Wessem, J. M., van de Berg, W. J., Noël, B. P. Y., van Meijgaard, E., Amory, C., Birnbaum, G., ... van den Broeke, M. R. (2018, apr). Modelling the climate and surface mass balance of polar ice sheets using RACMO2 – Part 2: Antarctica (1979–2016). *The Cryosphere*, *12*(4), 1479–1498. Retrieved from https://www.the-cryosphere-discuss.net/tc-2017-202/https://

www.the-cryosphere.net/12/1479/2018/ doi: 10.5194/tc-12-1479-2018

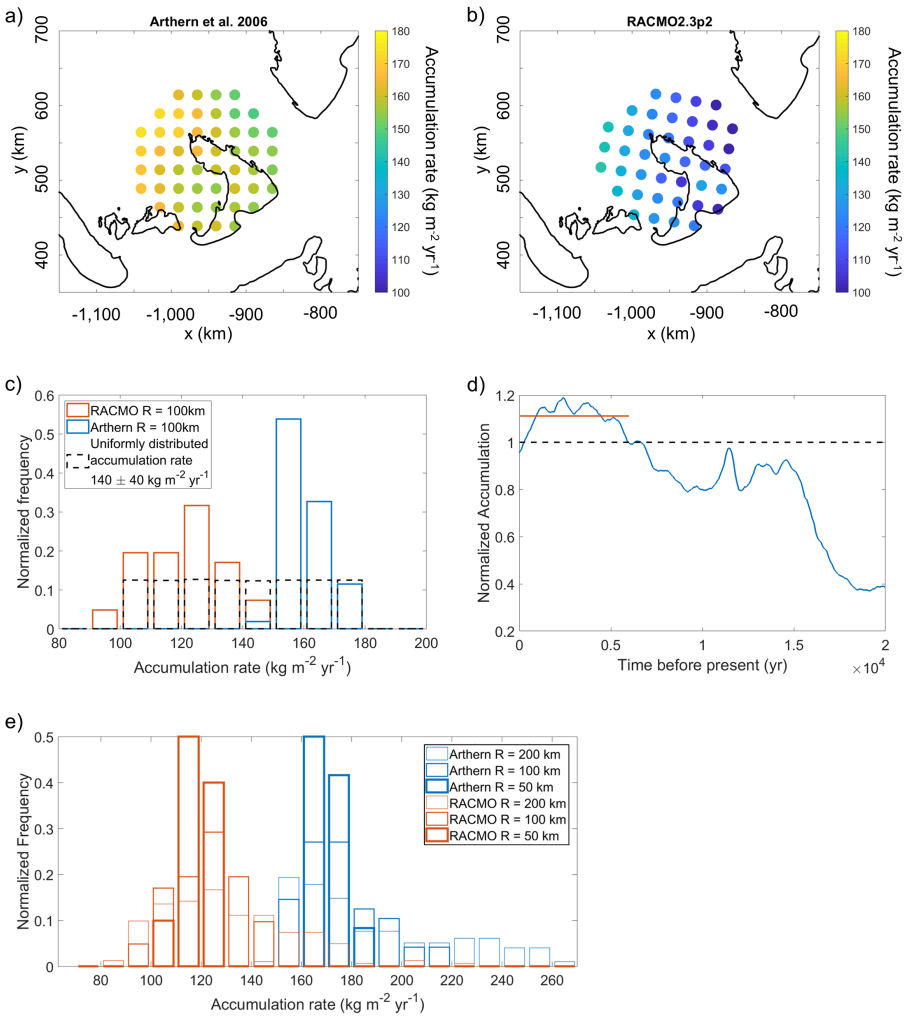

Figure 1. Accumulation rates within 100 km radius of the radar survey over HIR, from (a) from Arthern et al. (2006) and (b) RACMO2.3p2 from van Wessem et al. (2018). (c) Normalized frequency distribution in accumulation rates, with uniformly distributed accumulation rate designed to cover the range of values (blacked dashed bars) centred on 140 kg m^{-2} yr^{-1} (0.153 m yr^{-1}) with range ± 40 kg m^{-2} yr^{-1} (0.044 m yr^{-1}). (d) Accumulation record from WAIS Divide ice core (WDC) (Koutnik et al., 2016) normalized to mean accumulation within past 500 yr; averaged over past 6 kyr (red). (e) Accumulation rate downstream of DIR for 50, 100 and 200 km radii. The median 165 kg m^{-2} yr^{-1} (0.18 m yr^{-1}).

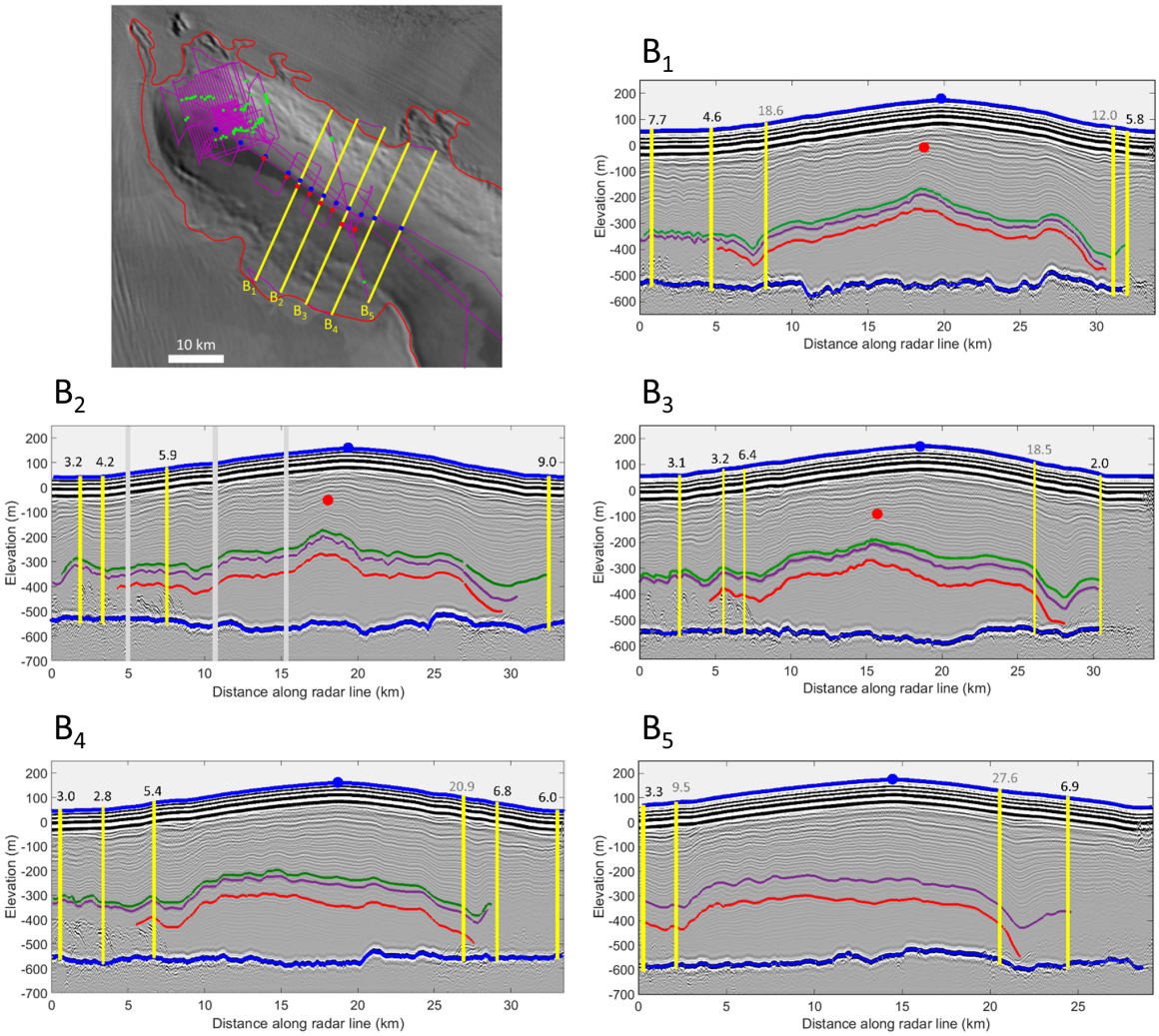

Figure 2. Radar profiles traversing the ice-divide between the West and East Flanks of HIR. The ice-divide is marked with blue circles, while the locations of low amplitude arches are denoted with red circles, if present. Arches become less developed and more offset towards the south, with under-developed arches absent in the two most southerly profiles. Yellow vertical lines mark locations where age estimates have been calculated for the grounding of these points; the mean age is given in kyr from 20,000 runs of the Monte-Carlo simulation. Age estimates in grey indicate that the dating was likely significantly affected by melting as is evident from the down-warped isochrones. In line B_2 areas with no data are marked by vertical grey bars.

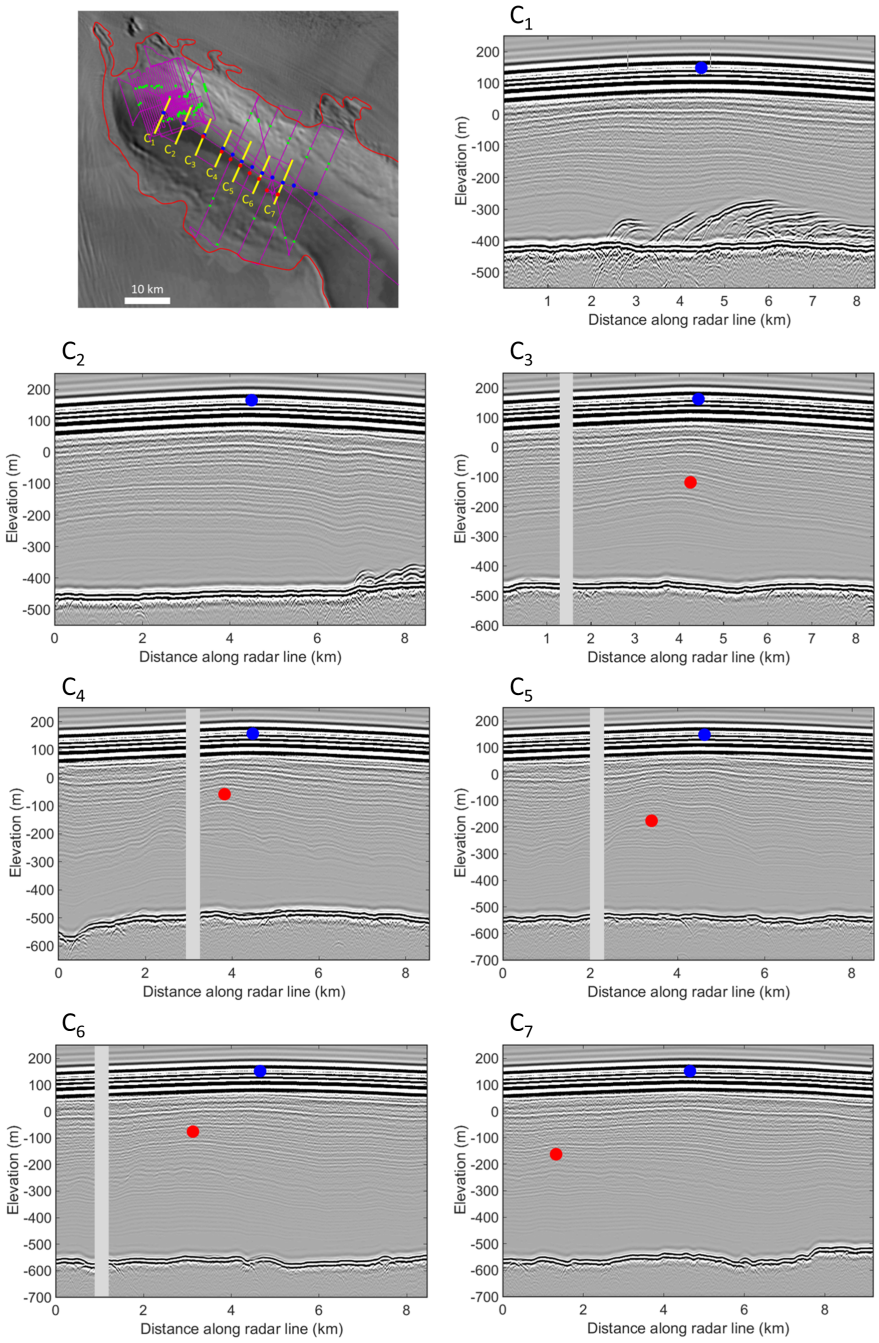

Figure 3. Seven radar profiles that traverse and are perpendicular-to the ice divide. The ridge is marked with blue circles and under-developed arches (as determined by eye) are marked with red circles. Areas with no data are indicated with vertical grey bars.

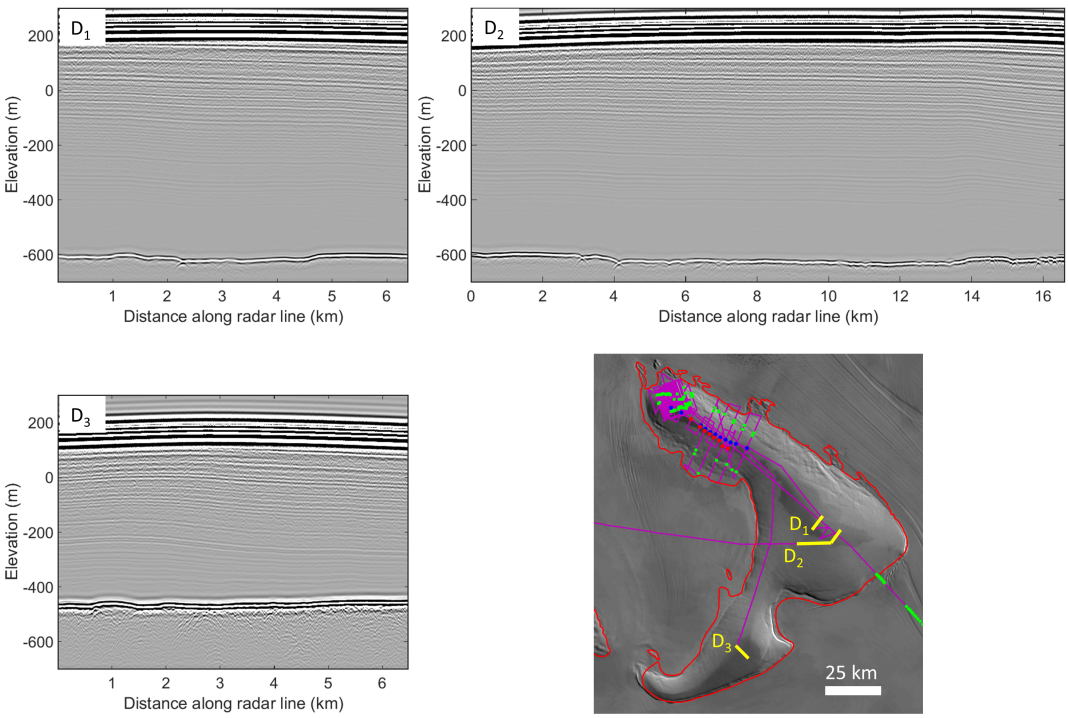

Figure 4. Radar profiles over ice-divides in southern sections of HIR, with location map. No evidence of Raymond Arches.

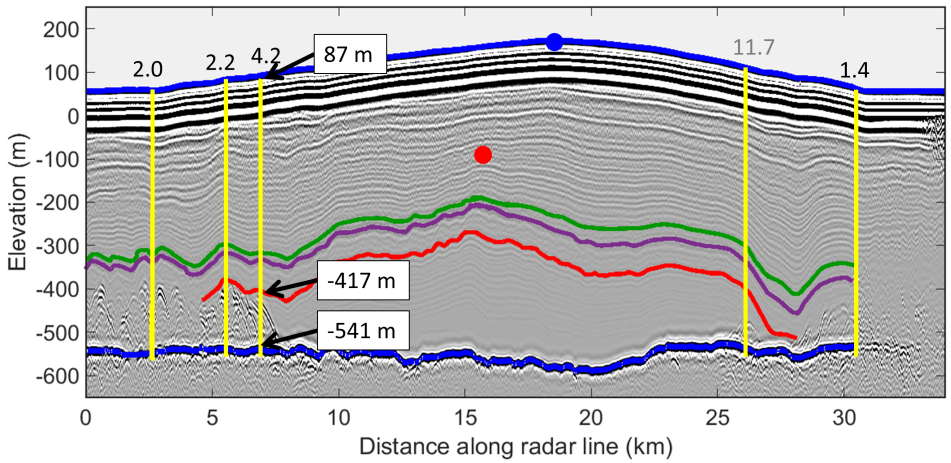

Figure 5. Radar line B_3 across ice divide, with bed elevation, relic crevasse height and surface height marked at location where the age of the relic basal crevasse is calculated.

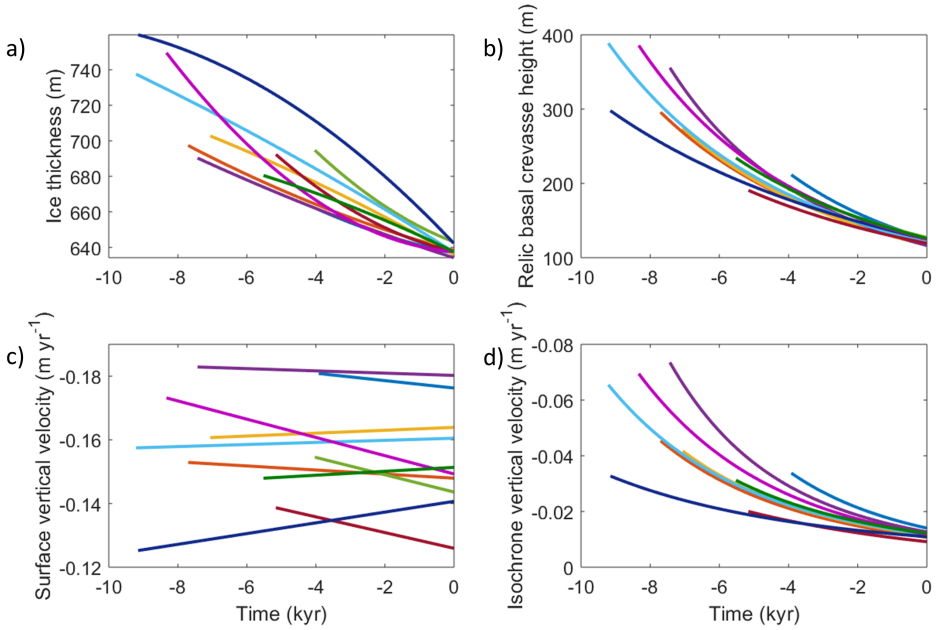

Figure 6. Ten runs of the Monte-Carlo simulation for the deformation of basal crevasses once grounded; (a) Evolution of ice thickness, from flotation thickness at grounding to present day. (b) Evolution of height of basal crevasse. (c) Vertical velocity at the ice surface. (d) Vertical velocity of isochrone that caps basal crevasse. Colour of curves corresponds to the same simulation across all plots.

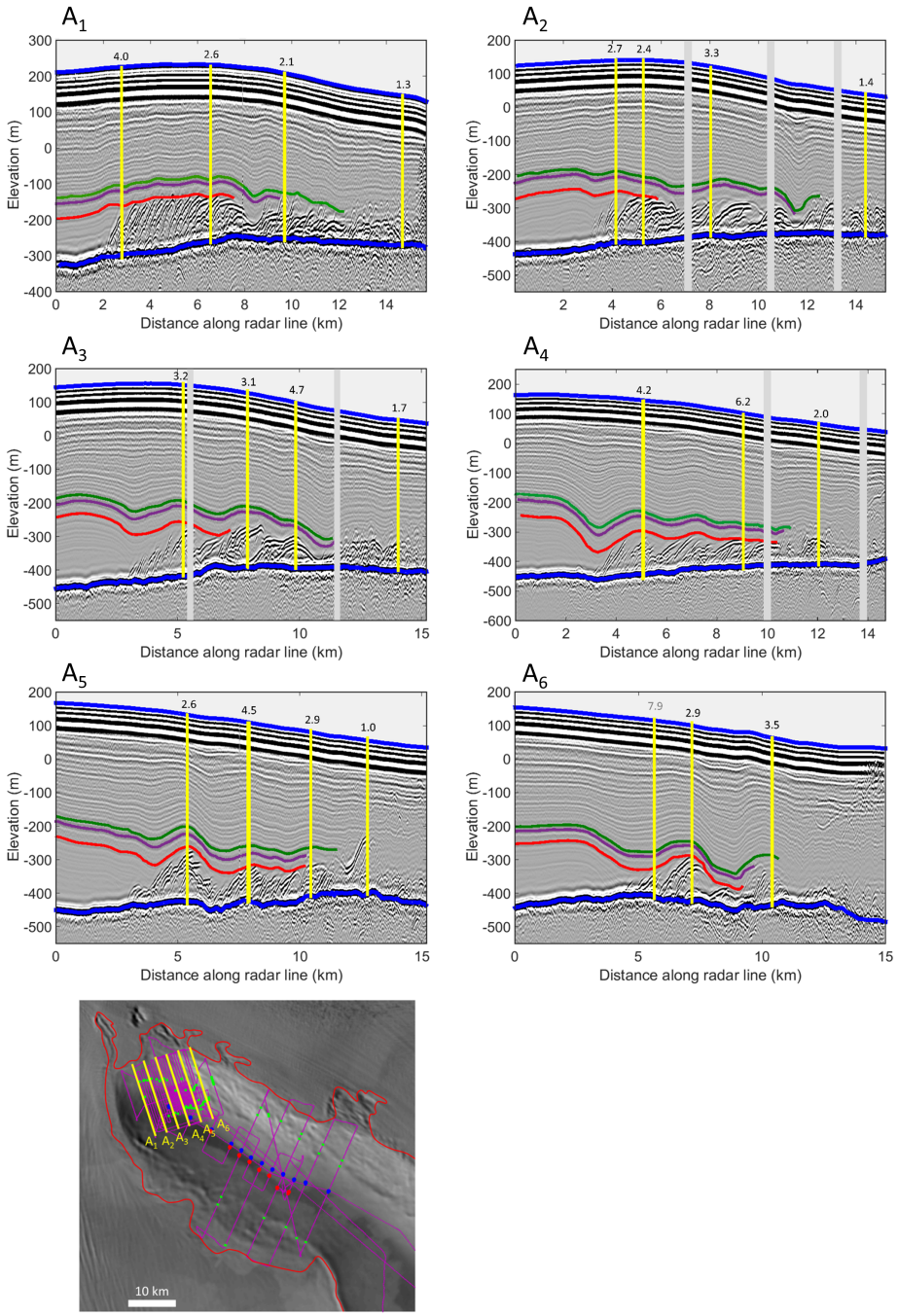

Figure 7. Six parallel radar profiles over the northern promontory, aligned approximately North-South, with locations shown in lower left map. In each panel the ice surface (blue), base (blue) and three capping isochrones (red, purple, green) are highlighted. Vertical yellow lines indicate where the age of grounding has been calculated, with mean estimated age given in kyr. Grey age estimates are assigned to locations where melting is evident and expected to have significantly affected the age estimate. Grey vertical bars indicate data gaps.

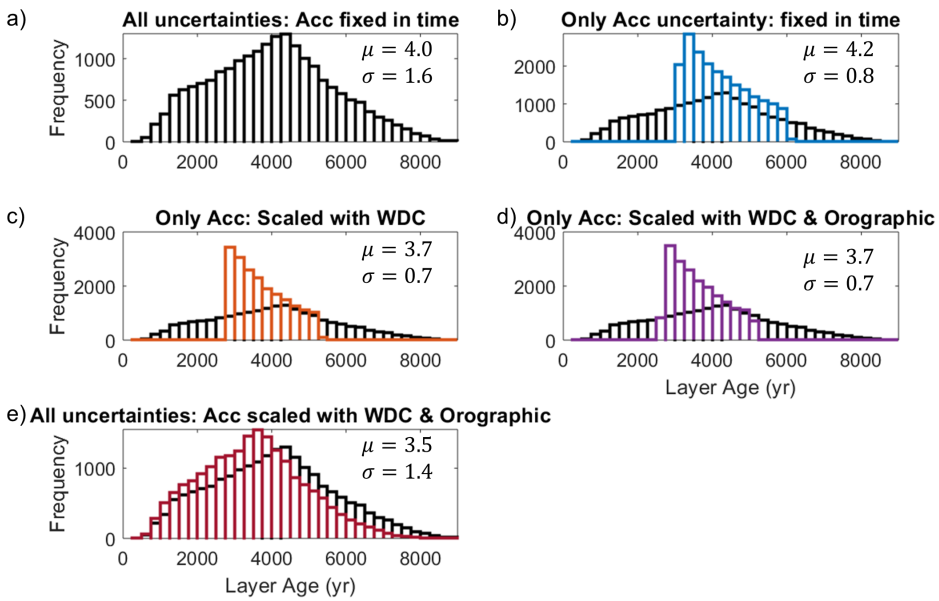

Figure 8. Age estimates for the most upstream basal crevasse on line A_1, with varying parameterizations of accumulation. (a) Uncertainties in all parameters are considered and accumulation is fixed in time corresponding to present-day accumulation. (b) Only the uncertainty in present-day accumulation is considered and this is fixed in time. (c) Only uncertainty in accumulation rate is consider, but it is allowed to vary in time, scaled by the WAIS Divide ice core (WDC). (d) Same as (c) but orographic effects are also considered; accumulation decreases by 4% per 100 m elevation gain. (e) All uncertainties are considered with accumulation varying with WDC and orographic effect.

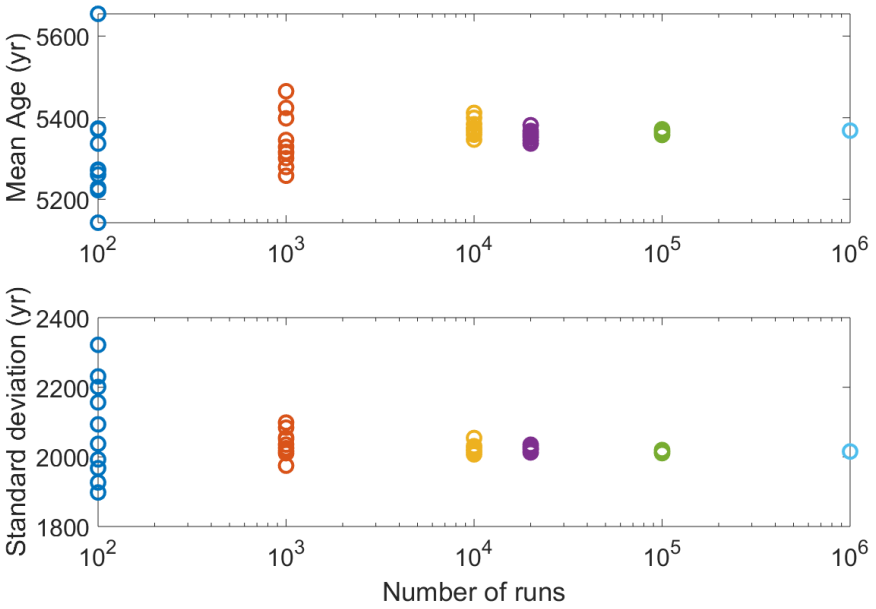

Figure 9. Mean age and standard deviation of age estimates from calculations using a Monte Carlo approach, with a varying number of runs included. Methodology is outlined in main text.